



A New Technology for Ac-Side Cascaded H-Bridge Cells for Multi-Level VSC-HVDC Transmission System

Authors

M.Srinath¹ Mr. G. Hari Krishna², M.Nagaraju³

¹PG Student [EPS], Dept. of EEE, ASIT, Gudur, SPSR Nellore (D), Andhra Pradesh, India

²Assistant Professor, Dept. of EEE, ASIT, Gudur, SPSR Nellore (D), Andhra Pradesh, India

³Associate Professor, Dept. of EEE, ASIT, Gudur, SPSR Nellore (D), Andhra Pradesh, India

Abstract

The VSC based HVDC transmission system offers the operational flexibility in terms of active and reactive power control, in addition to improved AC fault ride-through capability. The proposed converter offers a unique feature of DC fault blocking capability (ability to block power exchange between the AC and DC sides during the dc faults, hence no current flows in converter switches). This feature may eliminate the need for a DC-side circuit breaker in applications such as DC power transmission systems. This converter also offers the features available from the modular multilevel converter, such as AC fault ride-through capability, low conversion losses, low harmonic filtering requirement, and extension to a high number of levels without compromising capacitor voltage balancing.

To illustrate the feasibility of the proposed HVDC system, this project assesses its dynamic performance during steady-state and network alterations, including its response to AC and DC side faults. Long extra high voltage (EHV) AC lines cannot be loaded to their thermal limits in order to keep sufficient margin against transient instability. No alterations of conductors, insulator strings, and towers of the original line are needed.

Index Terms—DC fault reverse blocking capability, hybrid multilevel converter with ac side cascaded H-bridge cells, modular multilevel converter, voltage-source-converter high-voltage dc (VSCHVDC) transmission system.

I. INTRODUCTION

MULTILEVEL converters are finding increased attention in industry and academia as one of the preferred choices of electronic power conversion for high-power applications ^{[1]-[10]}. They have successfully made their way into the industry and therefore can be considered a mature and proven technology. Currently, they are commercialized in standard and customized products that power a wide range of applications, such as compressors, extruders, pumps, fans, grinding mills, rolling mills, conveyors, crushers, blast furnace blowers, gas turbine starters, mixers, mine hoists, reactive power compensation, marine propulsion, high-

voltage direct-current (HVDC) transmission, hydropumped storage, wind energy conversion, and railway traction, to name a few ^{[1]-[10]}. Converters for these applications are commercially offered by a growing group of companies in the field ^{[11]-[26]}. Although it is an enabling and already proven technology, multilevel converters present a great deal of challenges, and even more importantly, they offer such a wide range of possibilities that their research and development is still growing in depth and width. Researchers all over the world are contributing to further improve energy efficiency, reliability, power density, simplicity, and cost of multilevel converters, and broaden their

application field as they become more attractive and competitive than classic topologies. Recently, many publications have addressed multilevel converter technology and stressed the growing importance of multilevel converters for high-power applications [4]-[9]. These works have a survey and tutorial nature and cover in depth traditional and well-established multilevel converter topologies, such as the neutral point clamped (NPC), cascaded H-bridge (CHB), and flying capacitor (FC), as well as the most used modulation methods. Instead, this paper presents a technology review, which is focused mainly on the most recent advances made in this field in the past few years, covering new promising topologies, modulations, controls, and operational issues. In addition,

one of the most interesting topics in multilevel converter technology is the rapidly increasing and diverse application field, which is addressed in this work as well. In addition, emerging trends, challenges, and possible future directions of the development in multilevel converter technology are outlined to motivate further work in this field. With increased demand for clean energy, power system networks need to be reengineered to be more efficient and flexible and reinforced to accommodate increased penetration of renewable power without compromising system operation and reliability. A VSC-HVDC transmission system is a candidate to meet these challenges due to its operational flexibility, such as provision of voltage support to ac networks, its ability to operate independent of ac network strength therefore makes it suitable for connection of weak ac networks such as offshore wind farms, suitability for multiterminal HVDC network realization as active power reversal is achieved without dc link voltage polarity change, and resiliency to ac side faults (no risk of commutation failure as with line-commutating HVDC systems) [12],[16]-[22]. However, vulnerability to dc side faults and absence of reliable dc circuit breakers capable of operating at high-voltage restrict their application to point-to-

point connection. Present VSC-HVDC transmission systems rely on their converter station control systems and effective impedance between the point-of-common-coupling (PCC) and the converter terminals to ride-through dc side faults. With present converter technology, the dc fault current comprises the ac networks contribution through converter free-wheeling diodes and discharge currents of the dc side capacitors (dc link and cable distributed capacitors) [23],[24]. The magnitude of the dc-side capacitors' discharge current decays with time and is larger than the ac networks contribution. For this reason, dc fault interruption may require dc circuit breakers that can tolerate high let-through current that may flow in the dc side during the first few cycles after the fault, with high current breaking capacity and fast interruption time. Recent HVDC converter topologies with no common dc link capacitors, such as the modular multilevel converter (M2C), may minimize the magnitude and duration of the discharge current first peak [2],[12],[14],[23],[25]. There are two approaches to assist VSC-HVDC transmission systems to ride-through dc side faults. The first approach is to use a fast acting dc circuit breaker, with considerably high let-through current to tolerate the high dc fault discharge current that may flow in the dc side. This breaker must be capable of operating at high voltage and isolates temporary or permanent dc faults, plus have a relatively high-current-breaking capacity. Reference [26] presents a prototype 80-kV dc circuit breaker with dc current breaking capacity of 9 kA within 2ms. However, this first step is inadequate, as the operating voltage of present

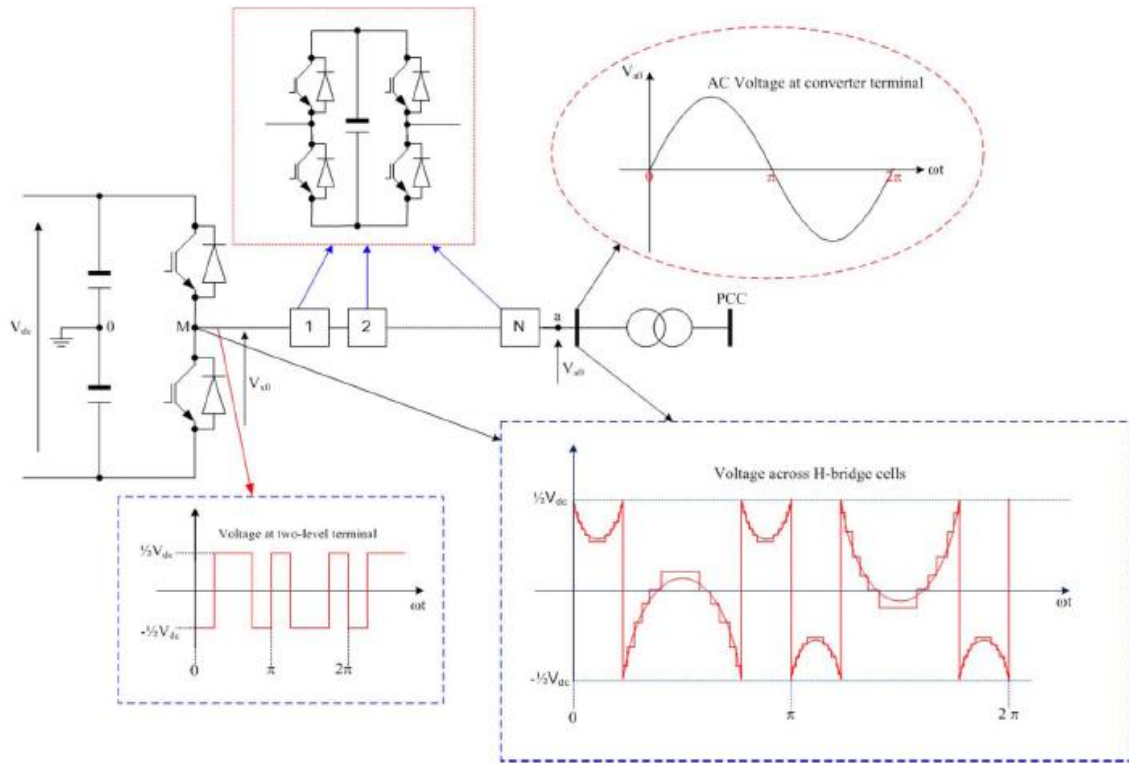


Fig. 1. Hybrid voltage multilevel converter with ac side cascaded H-bridge cells.

VSC-HVDC transmission systems reach 640 kV pole-to-pole (or 320 kV for a bi-polar configuration), with power-handling capability of 1 GW. This breaker approach may introduce significant steady-state losses due to the semiconductors in the main current path. The second approach is to use converter stations with dc fault reverse-blocking capability [1], [4], [23]. Each converter station must be able to block current flow between the ac and dc sides during a dc fault, allowing dc-side capacitor discharge current, which is the major component of the dc fault current, to decay to zero and then isolate the fault. Several converter topologies with this inherent feature have been proposed, including an H-bridge modular multilevel converter, an alternative arm modular multilevel converter, and a hybrid multilevel converter with ac-side cascaded H-bridge cells. However, the drawback is that the active power exchange between the ac networks reduces to zero during the dc fault period. Commensurate with the second approach, this paper presents a new HVDC transmission systems based on a hybrid-voltage-source multilevel

converter with ac-side cascaded H-bridge cells. The adopted converter has inherent dc fault reverse-blocking capability, which can be exploited to improve VSC-HVDC resiliency to dc side faults. With coordination between the HVDC converter station control functions, the dc fault reverse-blocking capability of the hybrid converter is exploited to achieve the following:

- eliminate the ac grid contribution to the dc fault, hence minimizing the risk of converter failure due to uncontrolled over current during dc faults;
- facilitate controlled recovery without interruption of the VSC-HVDC system from dc-side faults without the need for opening ac-side circuit breakers;
- simplify dc circuit breaker design due to a reduction in the magnitude and duration of the dc fault current; and
- improve voltage stability of the ac networks as converter reactive power consumption is reduced during dc-side faults.

Section II of this paper describes the operational principle and control of the hybrid voltage source multilevel converter with ac-side cascaded H-

bridge cells. Section III describes the HVDC system control design, specifically, ac current controller in synchronous reference frame, dc link voltage, and active power, and ac voltage controllers. A detailed block diagram that summarizes how different control layers of the proposed HVDC transmission system are interfaced is presented. Section IV presents simulations of a hybrid converter HVDC transmission system, which demonstrate its response during steady-state and network disturbances. Included are simulations of four quadrant operation, voltage support capability, and ac and dc fault ride-through capabilities.

II. HYBRID MULTILEVEL VSC WITH AC-SIDE CASCADED H-BRIDGE CELLS

Fig. 1 shows one phase of a hybrid multilevel VSC with H-bridge cells per phase. It can generate voltage levels at converter terminal “a” relative to supply midpoint “0.” Therefore, with a large number of cells per phase, the converter presents near pure sinusoidal voltage to the converter transformer as depicted in Fig. 1^[1]. The two-level converter that blocks high-voltage controls the fundamental voltage using selective harmonic elimination (SHE) with one notch per quarter cycle, as shown in Fig. 1. Therefore, the two-level converter devices operate with 150-Hz switching losses, hence low switching losses and audible noise are expected. The H-bridge cells between “M” and “a” are operated as a series active power filter to attenuate the voltage harmonics produced by the two-level converter bridge. These H-bridge cells are controlled using level-shifted carrier-based multilevel pulsewidth modulation with a 1-kHz switching frequency. To minimize the conversion losses in the H-bridge cells, the number of cells is reduced such that the voltage across the H-bridge floating capacitors sum to. This may result in a small converter station, because the number of H-bridge cells required per converter with the proposed HVDC system is one quarter of those required for a system based on the modular multilevel converter.

With a large number of cells per phase, the voltage waveform generated across the H-bridge cells is as shown in Fig. 1, and an effective switching frequency per device of less than 150 Hz is possible. The dc fault reverse-blocking capability of the proposed HVDC system is achieved by inhibiting the gate signals to the converter switches, therefore no direct path exists between the ac and dc side through freewheel diodes, and cell capacitor voltages will oppose any current flow from one side to another. Consequently, with no current flows, there is no active and reactive power exchange between ac and dc side during dc-side faults. This dc fault aspect means transformer coupled H-bridges cannot be used. The ac grid contribution to dc-side fault current is eliminated, reducing the risk of converter failure due to increased current stresses in the switching devices during dc-side faults. From the grid standpoint, the dc fault reverse-blocking capability of the proposed HVDC system may improve ac network voltage stability, as the reactive power demand at converter stations during dc-side faults is significantly reduced. The ac networks see the nodes where the converter stations are connected as open circuit nodes during the entire dc fault period. However, operation of the hybrid multilevel VSC requires a voltage-balancing scheme that ensures that the voltages across the H-bridge cells are maintained at under all operating conditions, where is the total dc link voltage. The H-bridge cells voltage balancing scheme is realized by rotating the H-bridge cell capacitors, taking into account the voltage magnitude of each cell capacitor and phase current polarity. An additional PI regulator is used to ensure that the cell capacitors be maintained at as depicted in Fig. 2(b) (inner control layer).

III. CONTROL SYSTEMS

A HVDC transmission system based on a hybrid multilevel VSC with ac-side cascaded H-bridge cells requires three control system layers. The inner control layer represents the modulator and

capacitor voltage-balancing mechanism that generates the gating signals for the converter switches and maintains voltage balance of the H-bridge cell capacitors. The intermediate control layer represents the current controller that regulates the active and reactive current components over the full operating range and restrains converter station current injection into ac network during network disturbances such as ac and dc side faults. The outer control layer is the dc voltage (or active power) and ac voltage (or reactive power) controller that provide set points to the current controllers. The inner controller has only been discussed to a level appropriate to power systems engineers. The intermediate and outer control layers are presented in detail to give the reader a sense of HVDC control system complexity. The current, power, and dc link $\lambda_d = V_{cd} - V_d + \omega L i_q$ and $\lambda_q = V_{cq} - V_q - \omega L i_d$

$$\frac{di_d}{dt} = -\frac{R}{L} i_d + \frac{1}{L} \lambda_d \quad (3)$$

$$\frac{di_q}{dt} = -\frac{R}{L} i_q + \frac{1}{L} \lambda_q \quad (4)$$

The new control variables and can be obtained from two proportion-integral controllers (PI) having the same gains:

$$\lambda_d = K_p (i_d^* - i_d) + K_i \int (i_d^* - i_d) dt \quad (5)$$

$$\lambda_q = K_p (i_q^* - i_q) + K_i \int (i_q^* - i_q) dt \quad (6)$$

where and represent reference direct and quadrature current components.

To facilitate control design in state space, the integral parts of λ_d and λ_q are replaced by

$W_d = K_i \int (i_d^* - i_d) dt$ and $W_q = K_i \int (i_q^* - i_q) dt$, rearranged in the following form:

$$\lambda_d = K_p (i_d^* - i_d) + W_d \quad (7)$$

$$\lambda_q = K_p (i_q^* - i_q) + W_q \quad (8)$$

The integral parts, in differential equations form, are

$$\frac{dW_d}{dt} = -K_i i_d + K_i i_d^* \quad (9)$$

$$\frac{dW_q}{dt} = -K_i i_q + K_i i_q^* \quad (10)$$

After substitution of (7) and (8) into (3) and (4), two identical and independent sets of equations, suitable for control design, are obtained as

voltage controller gains are selected using root locus analysis, based on the applicable transfer functions. Some of the controller gains obtained using root locus analysis give good performance in steady state but failed to provide acceptable network disturbance performance. Therefore, the simulation final gains used are adjusted in the time domain to provide satisfactory performance over a wide operating range, including ac and dc side faults. Fig. 2 summarizes the control layers of the hybrid multilevel VSC. *Current Controller Design:* The differential equations describing the ac-side transient and steady-state are

$$\frac{di_d}{dt} = -\frac{R}{L} i_d + \frac{1}{L} (V_{cd} - V_d + \omega L i_q) \quad (1)$$

$$\frac{di_q}{dt} = -\frac{R}{L} i_q + \frac{1}{L} (V_{cq} - V_q + \omega L i_d) \quad (2)$$

Assume

$$\begin{bmatrix} \frac{di_d}{dt} \\ \frac{dW_d}{dt} \end{bmatrix} = \begin{bmatrix} -\frac{(R+K_p)}{L} & \frac{1}{L} \\ -K_i & 0 \end{bmatrix} \begin{bmatrix} i_d \\ W_d \end{bmatrix} + \begin{bmatrix} \frac{K_p}{L} \\ \frac{K_i}{K_i} \end{bmatrix} i_d^* \quad (11)$$

$$\begin{bmatrix} \frac{di_q}{dt} \\ \frac{dW_q}{dt} \end{bmatrix} = \begin{bmatrix} -\frac{(R+K_p)}{L} & \frac{1}{L} \\ -K_i & 0 \end{bmatrix} \begin{bmatrix} i_q \\ W_q \end{bmatrix} + \begin{bmatrix} \frac{K_p}{L} \\ \frac{K_i}{K_i} \end{bmatrix} i_q^* \quad (12)$$

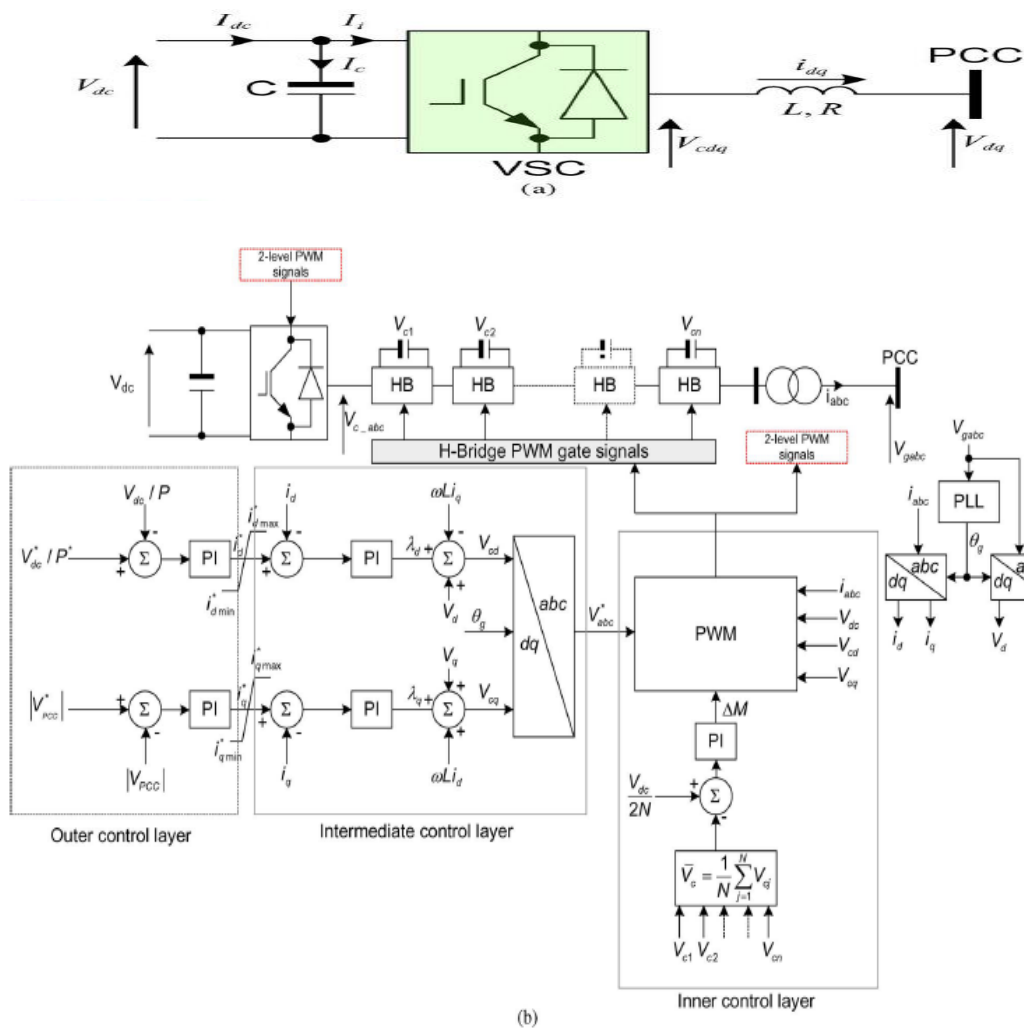


Fig. 2. (a) Representation of VSC station and (b) schematic diagram summarizing the control layer of the hybrid multilevel converter with ac side cascaded H-bridge cells

After Laplace manipulations of the state-space equations in (11) and (12), one transfer function is obtained for and , which is used for the current controller design

$$\frac{i_d(s)}{i_d^*(s)} = \frac{i_q(s)}{i_q^*(s)} = \frac{\frac{K_p}{L}s + \frac{K_i}{L}}{s^2 + \frac{(R + K_p)}{L}s + \frac{K_i}{L}}$$

Equations relating the reference voltages to the modulator and , current controller output, and feedforward terms can be obtained from expressions for and as follows: $V_{cd}^* = \lambda_d + V_d - \omega L i_q$ (13)

$$V_{cq}^* = \lambda_q + V_q + \omega L i_d \quad (14)$$

Based on (5), (6), (13), and (14), the structure of the current controller shown in Fig. 2(b) (intermediate layer) is obtained. **DC Voltage Controller:** Based on Fig. 2, the differential

equation describing the converter dc-side dynamics is

$$C \frac{dv_{dc}}{dt} = I_{dc} - I_i \quad (15)$$

Assuming a lossless VSC, dc power at the converter dc link must equal the ac power at converter terminal $I_i = \frac{(v_{cd} i_d + v_{cq} i_q)}{V_{dc}}$.

Therefore, (15) can be written as

$$C \frac{dv_{dc}}{dt} = I_{dc} - \frac{(v_{cd} i_d + v_{cq} i_q)}{V_{dc}} \quad (16)$$

Equation (16) can be linearized using a Taylor series with the higher order terms neglected. Therefore, the linearized form of (16) is

$$\frac{d\Delta V_{dc}}{dt} = \frac{\Delta I_{dc}}{C} - \frac{v_{cd}}{C V_{dc}} \Delta i_d - \frac{v_{cq}}{C V_{dc}} \Delta i_q - \frac{i_d}{C V_{dc}} \Delta V_{cd} - \frac{i_q}{C V_{dc}} \Delta V_{cq} + \frac{(v_{cd} i_d + v_{cq} i_q)}{C V_{dc}^2} \Delta V_{dc} \quad (17)$$

$$\text{let } P_{ac} = V_{cd}i_d + V_{cq}i_q \quad \text{and} \quad \Delta u_{dc} = \Delta I_{dc} - \left(\frac{V_{cd}}{V_{dc}}\right)\Delta I_d - \left(\frac{V_{cq}}{V_{dc}}\right)\Delta I_q - \left(\frac{i_d}{V_{dc}}\right)\Delta V_{cd} - \left(\frac{i_q}{V_{dc}}\right)\Delta V_{cq}$$

and the variable Δu_{dc} can be obtained from the DC voltage controller based on the PI control as follows:

$$\Delta u_{dc} = K_{pdc}(\Delta V_{dc}^* - \Delta V_{dc}) + \int (\Delta V_{dc}^* - \Delta V_{dc}) dt \quad (18)$$

Equation (17) can be reduced to

$$\frac{d\Delta V_{dc}}{dt} = \frac{\Delta u_{dc}}{c} + \frac{P_{ac}}{cv_{dc}^2} \Delta V_{dc} \quad (19)$$

where represents reference dc link voltage. Let the new control variable introduced for the integral part of the dc voltage controller be , therefore:

$$\frac{d\Delta V_{dc}}{dt} = -\frac{1}{c} \left(K_{pdc} - \frac{P_{ac}}{v_{dc}^2} \right) \Delta V_{dc} + \frac{1}{c} \Delta Z_{dc} + \frac{\Delta V_{dc}^*}{c} \quad (20)$$

$$\frac{d\Delta Z_{dc}}{dt} = K_{idc} (\Delta V_{dc}^* - \Delta V_{dc}) \quad (21)$$

The state equations in (20) and (21) in matrix form are:

$$\frac{d}{dt} \begin{bmatrix} \Delta V_{dc} \\ \Delta Z_{dc} \end{bmatrix} = \begin{bmatrix} -\left(\frac{K_{pdc}}{c} - \frac{P_{ac}}{cv_{dc}^2}\right) & \frac{1}{c} \\ -K_{idc} & 0 \end{bmatrix} \begin{bmatrix} \Delta V_{dc} \\ \Delta Z_{dc} \end{bmatrix} + \begin{bmatrix} \frac{K_{pdc}}{c} \\ K_{idc} \end{bmatrix} \Delta V_{dc}^* \quad (22)$$

Equation (22) in the s-domain is

$$\begin{bmatrix} \Delta V_{dc}(s) \\ \Delta Z_{dc}(s) \end{bmatrix} = \frac{1}{\Gamma} \begin{bmatrix} s & \frac{1}{c} \\ -K_{idc} & s + \left(\frac{K_{pdc}}{c} - \frac{P_{ac}}{cv_{dc}^2}\right) \end{bmatrix} \begin{bmatrix} \frac{K_{pdc}}{c} \\ K_{idc} \end{bmatrix} \Delta V_{dc}^* \quad (23)$$

where $\Gamma = s^2 + \left(\frac{K_{pdc}}{c} - \frac{P_{ac}}{cv_{dc}^2}\right)s + \frac{K_{idc}}{c}$

$$\begin{bmatrix} \Delta V_{dc}(s) \\ \Delta Z_{dc}(s) \end{bmatrix} = \begin{bmatrix} \frac{\frac{K_{pdc}}{c}s + \frac{K_{idc}}{c}}{s^2 + \left(\frac{K_{pdc}}{c} - \frac{P_{ac}}{cv_{dc}^2}\right)s + \frac{K_{idc}}{c}} \\ \frac{K_{idc} \left(s - \frac{P_{ac}}{cv_{dc}^2}\right)}{s^2 + \left(\frac{K_{pdc}}{c} - \frac{P_{ac}}{cv_{dc}^2}\right)s + \frac{K_{idc}}{c}} \end{bmatrix} \Delta V_{dc}^* \quad (24)$$

From (24), the transfer function for the dc voltage controller is

$$\frac{V_{dc}(s)}{V_{dc}^*(s)} = \frac{\frac{K_{pdc}}{c}s + \frac{K_{idc}}{c}}{s^2 + \left(\frac{K_{pdc}}{c} - \frac{P_{ac}}{cv_{dc}^2}\right)s + \frac{K_{idc}}{c}} \quad (25)$$

Normally, the voltage angle at the converter terminal relative to the PCC is sufficiently small, resulting in and . Therefore, the reference current for the current controller can be obtained from the outer dc voltage controller as follows:

$$\Delta I_{dc}^* = -\frac{1}{v_{cd}} (\Delta u_{dc} + i_d \Delta \bar{v}_{cd} - \Delta I_{dc}) \quad (26)$$

Active Power Controller: The active power controller sets the reference active current

component assuming a constant voltage at the PCC as follows:

$$i_d^* = K_{pp}(P^* - V_d^* i_d) + K_{ip} \int (P^* - V_d^* i_d) dt \quad (27)$$

Assume the voltage vector at the PCC is aligned with the -axis and its magnitude is regulated at as , and represents active power reference. After replacing the integral part with a new control variable , the following sets of equations result:

$$i_d^* = K_{pp}(P^* - V_d^* i_d) + Z_p \quad (28)$$

$$\frac{dZ_p}{dt} = K_{ip}(P^* - V_d^* i_d) \quad (29)$$

After substituting (28) into (11), the following state space representation for the power controller is obtained:

$$\begin{bmatrix} \frac{di_d}{dt} \\ \frac{dZ_d}{dt} \\ \frac{dZ_p}{dt} \end{bmatrix} = \begin{bmatrix} -\frac{(R + K_p + K_p K_{pp} V_d^*)}{L} & \frac{1}{L} & \frac{K_p}{L} \\ -(K_i + K_i K_{pp} V_d^*) & 0 & K_i \\ -K_{ip} V_d^* & 0 & 0 \end{bmatrix} \begin{bmatrix} i_d \\ Z_d \\ Z_p \end{bmatrix} + \begin{bmatrix} \frac{K_p K_{pp}}{L} \\ K_i K_{pp} \\ K_{ip} \end{bmatrix} P^*$$

where we have (30), shown at the bottom of the page. **AC Voltage Controller:** The reference reactive power current component is set by the ac voltage controller as

$$i_q^* = K_{pv} (|V_{ac}^*| - |V_{ac}|) + K_{iv} \int (|V_{ac}^*| - |V_{ac}|) dt$$

where represents reference voltage magnitude at PCC. However, the gains for the ac voltage controllers are obtained using a trial-and-error search method that automatically runs the overall system simulation several times in an attempt to find the gains that produce the best time domain performance. The gains for all of the controllers and test network parameters used in this paper are listed in Tables I–III.

$$\frac{P(s)}{P^*(s)} = V_d^* \times \frac{i_d(s)}{P^*(s)} = V_d^* \times \frac{\left(\frac{K_p K_{pp} + K_i K_{pp} + K_p K_{ip}}{L}\right) s + \frac{K_i}{L}}{s^3 + \frac{(R + K_p + K_p K_{pp} V_d^*)}{L} s^2 + \frac{(K_i + K_i K_{pp} V_d^* + K_p K_{ip} V_d^*)}{L} s + \frac{K_i K_{ip} V_d^*}{L}} \quad (30)$$

Table I Converter Stations Parameters

Converters 1 and 2		
Power ratings		687
Maximum active power capability	active power	MVA
Maximum reactive power capability	reactive power	600 MW 335Mvar
Two-level dc link voltage		600 KV
H-bridge dc link voltage		42.86KV
Two-level dc link capacitance		150 μ F
H-bridge cell capacitance		3mF
H-bridge switching frequency		1KHZ
Converter 1 controllers		35
Current controller:K _p		3000
Current controller k _i		0.0015
Power controller k _{pp}		20
Power controller k _{ip}		30
AC voltage controller k _{pV}		500
AC voltage controller k _{iV}		
Converter 2 controllers		38
Current controller:K _p		2000
Current controller k _i		0.015
DC voltage controller k _{pdc}		0.0573
DC voltage controller k _{idc}		0.00015
AC voltage controller k _{pV}		400
AC voltage controller k _{iV}		

A. Four-Quadrant Operation and Voltage Support

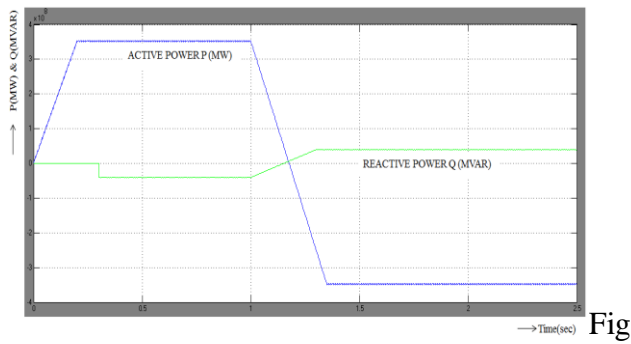
To demonstrate four-quadrant operation and voltage support capability of the presented VSC-HVDC system, converter station 1 is commanded to increase its output power export from grid to from 0 to 0.5 pu (343.5 MW) at 2.5 pu/s. At time 1 s it is commanded to reverse the active power flow in order to import 343.5 MW from grid, at 2.5 pu/s. At a load of is introduced to, illustrating the voltage support capability of converter station 2 during network alteration. Fig. 3(b) and (c) show converters 1 and 2 active and reactive power exchange with and respectively. The converters are able to adjust their reactive power exchange with and in order to support the voltage during the entire operating period. Fig. 3(c) and (d) show that converter 2 adjusts its reactive power exchange with when the load is introduced at 2 s to support the voltage magnitude. Fig. 3(e) and (f) show that

converter 2 injects and presents high-quality current and voltage waveforms into with no ac filters installed). Fig. 3(g) demonstrates that the voltage stresses across the H-bridge cell capacitors of converter 1 are controlled to the desired set point during the entire period. Fig. 3(h) displays the total dc link voltage across converter 2, which regulates the dc link voltage. Based on these results, the proposed VSC-HVDC system is able to meet basic steady-state requirements, such as provision of voltage support and four quadrant operation without compromising the voltage and current stresses on the converters switches.

B. AC Network Faults

To demonstrate the ac fault ride-through capability of the presented HVDC system, the test network is subjected to a 140 ms three-phase fault to ground at the location shown in Fig. 3(a). During the fault period the power command to converter 1 is reduced in proportion to the reduction in the ac voltage magnitude (this is achieved by sensing voltage). This is to minimize the two-level converter dc link voltage rise because of the trapped energy in the dc side, since power cannot be transferred as the voltage at collapses. Fig. 4 displays the results when the test network exports 0.5 pu (343.5 MW) from grid to and is subjected to the three-phase fault at t=1s. Fig. 4(a) shows the active and reactive powers converter 1 exchanges with. Note that converter 1 matches its active power export to in order to minimize the rise of converter 2 dc link voltage as its ability to inject active power into grid reduces with the voltage collapse at, as shown in Fig. 4(d) and stated above. Fig. 4(b) shows the active and reactive powers that converter 2 injects into. The system is able to recover as soon as the fault is cleared, and converter 2 adjusts its reactive power exchange with grid in order support voltage at [see Fig. 4(d)]. The transients shown of active and reactive powers at PCC2 are related to the reaction of the ac voltage controller that regulates the ac voltage at. Fig. 4(c) shows that the voltage

magnitude at remains unaffected; confirming that the hybrid voltage source



3(b)

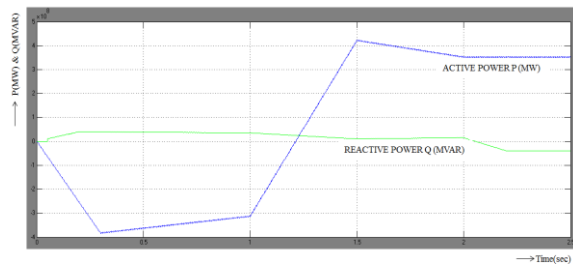


Fig 3(c)

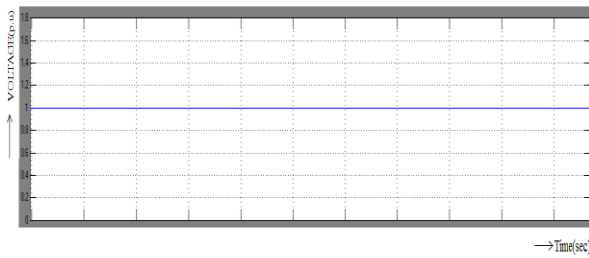


Fig 3(d)

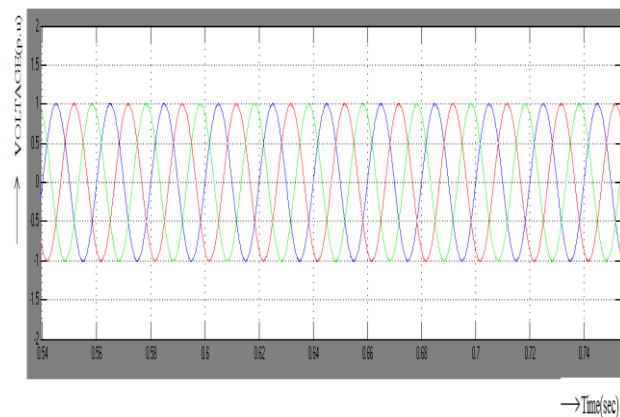


Fig 3(e)

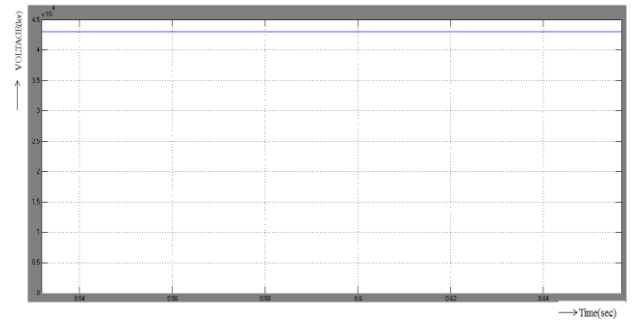


Fig 3(g)

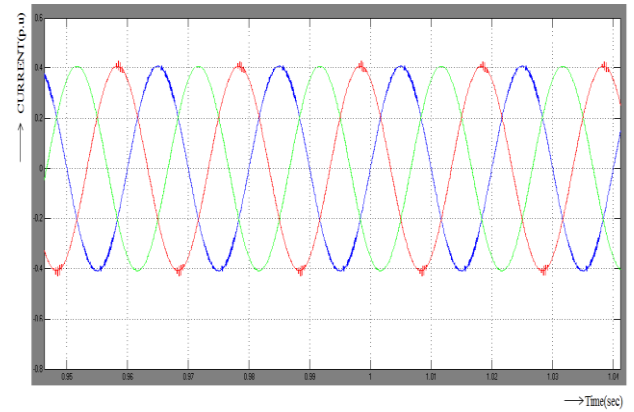


Fig 3(f)

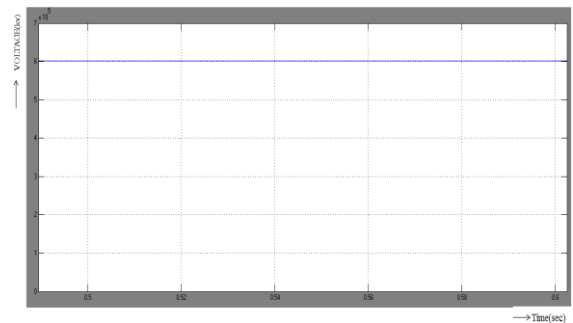


Fig 3(h)

Fig. 3. Test network and waveforms demonstrating the steady-state operation of HVDC system based on hybrid voltage source multilevel converter with ac side cascaded H-bridge cells. (a) Test network used to illustrate the viability of the hybrid multilevel voltage source converter HVDC systems; (b) active and reactive power converter station 1 exchanges with ; (c) active and reactive power converter station 2 exchanges with ; (d) voltage magnitude at ; (e) voltage waveforms at ; (f) current waveforms converter station 1 exchanges with ; (g) voltage across 21 cell capacitors of the three phases of converter 1; (h) voltage across the dc link of converter station 2.

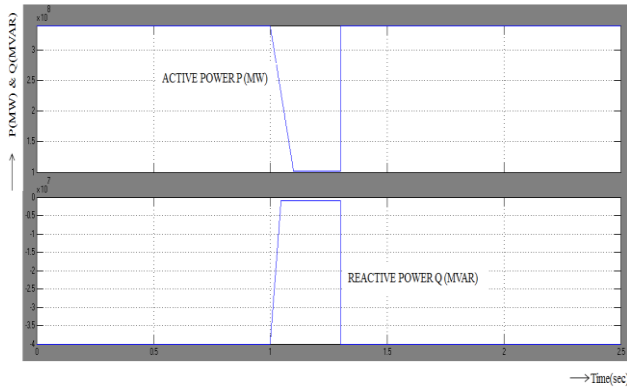


Fig 4(a)

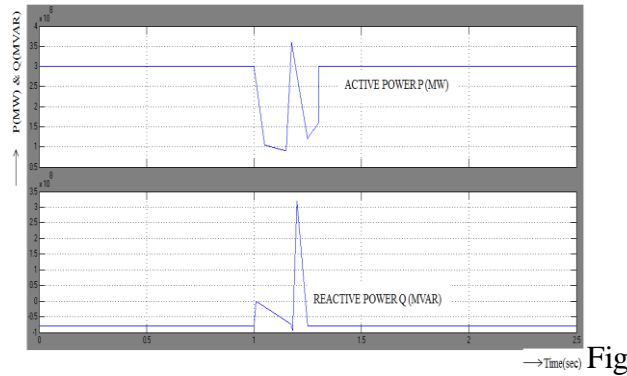


Fig 4(b)

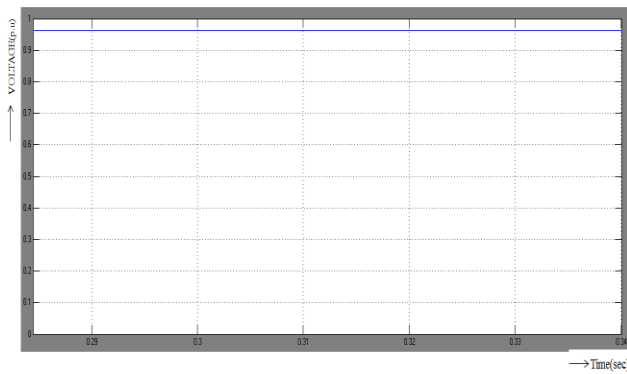


Fig 4(c)

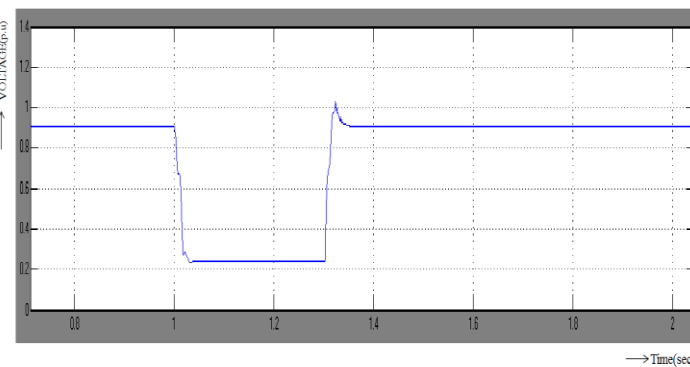


Fig 4(d)

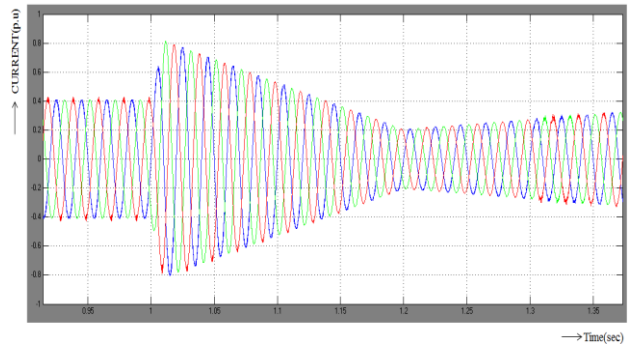


Fig 4(e)

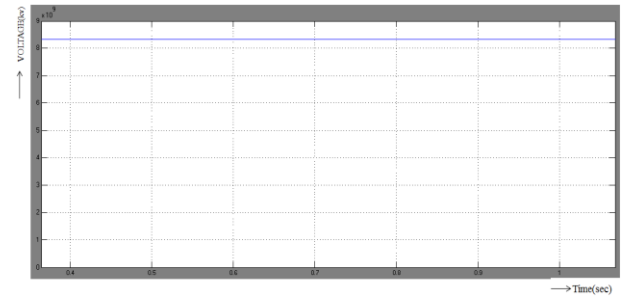


Fig 4(f)

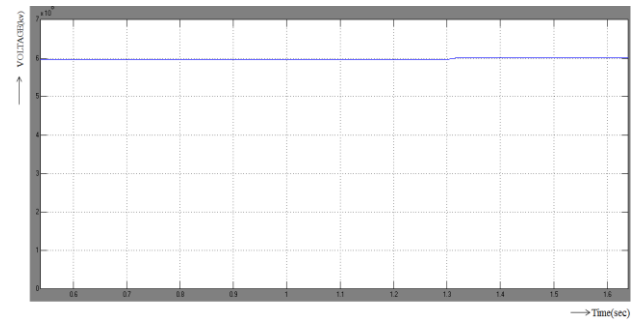


Fig 4(g)

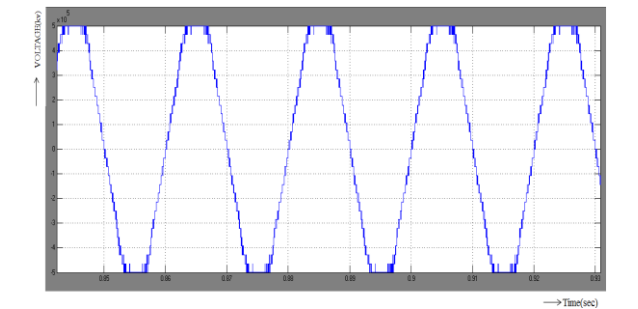


Fig 4(h)

Fig. 4. Waveforms demonstrating ac fault ride-through capability of HVDC transmission systems based on hybrid voltage multilevel converter with ac side cascaded H-bridge cells. (a) Active and reactive power converter 1 exchanges with . (b) Active and reactive power converter 2 injects into . (c) Voltage magnitude at . (d) Voltage magnitude

at . (e) Current waveforms converter 2 injects into . (f) Converter 2 dc link voltage. (g) Voltage across 21 H-bridge cells of the converter 2. (h) Line-to-line voltage waveform at the terminal of converter 1 (before transformer). (i) Active and reactive power at PCC1. (j) Active and reactive power at PCC2. Results in (i)–(o) demonstrate the case when the converter stations operate close to their maximum active power capabilities (power command at converter 1 is set to 0.75 pu, which is 515 MW) and system is subjected to a three-phase fault with a 300- ms duration.

multilevel converter does not compromise the HVDC transmission system's decoupling feature despite adopting active power matching at converter 1, as explained. Fig. 4(e) shows that converter 2 restrains its contribution to the fault current to less than full load current despite the voltage at collapsing to 20% of its rated voltage, due to converter 2's current controller. Fig. 4(f) shows that coordination of the HVDC controllers, as illustrated, minimizes the impact of ac-side faults on the transient power flow on the dc side, hence minimizing disturbance on the dc link voltage. Fig. 4(g) shows that the H-bridge cell voltage stresses are controlled as the system rides through the ac-side fault. This confirms that the complexity of a HVDC system based on the hybrid multilevel VSC does not compromise its ac fault ride-through capability. Fig. 4(h) shows the hybrid multilevel VSC presents high-quality voltage to the converter transformer, with low harmonic content and . This may permit elimination of ac-side filters and the use of standard insulation ac transmission transformers.

C. DC Network Faults

The inherent current-limiting capability of the hybrid multilevel VSC with ac-side cascaded H-bridge cells that permits the VSC-HVDC system to ride-through dc-side faults will be demonstrated here. The test network is subjected to a 140 ms solid pole-to-pole dc-side fault at the location indicated in Fig. 3(a). During the dc-side fault period, active power exchange between the two

grids and is reduced to zero. This facilitates uninterruptable system recovery from the temporary dc fault with minimal inrush current, since the power paths between the converter's ac and dc sides are blocked (by inhibiting all converter gate signals) to eliminate a grid contribution to the dc fault

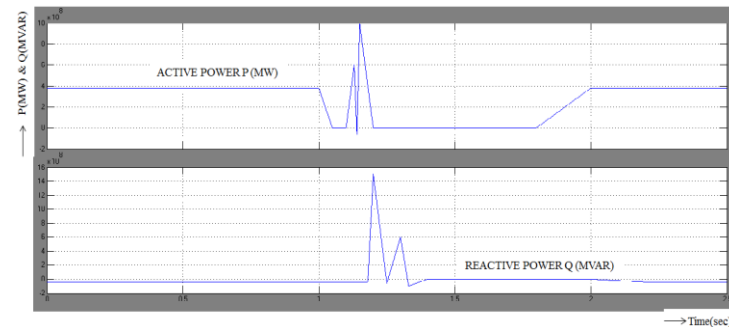


Fig 5 (a)

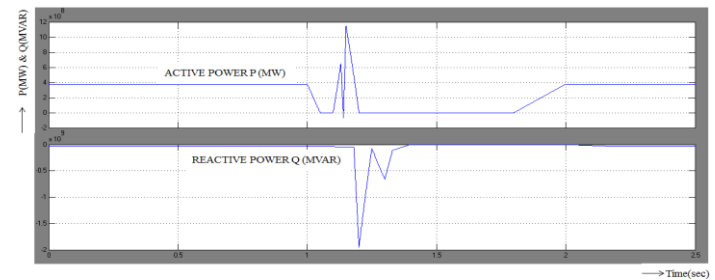


Fig 5 (b)

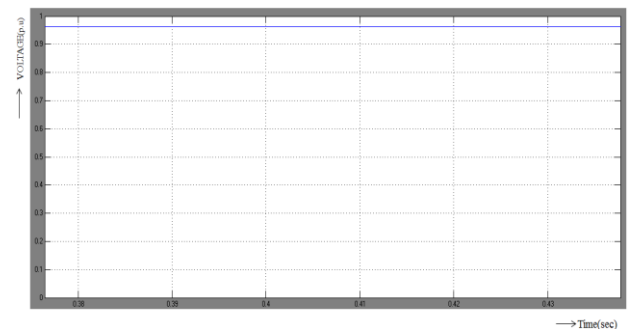


Fig 5 (c)

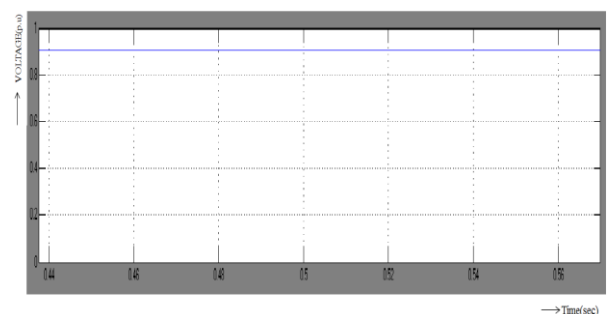


Fig 5 (d)

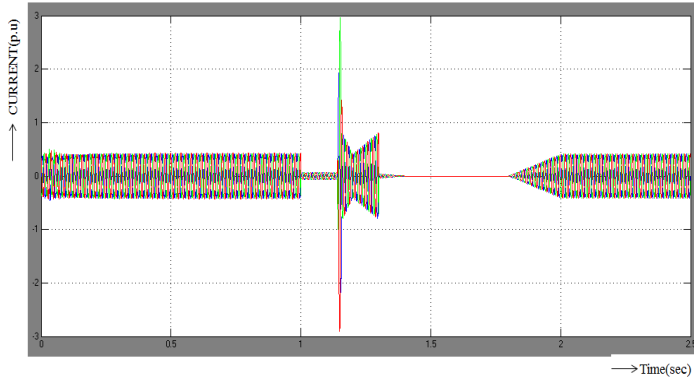


Fig 5(e)

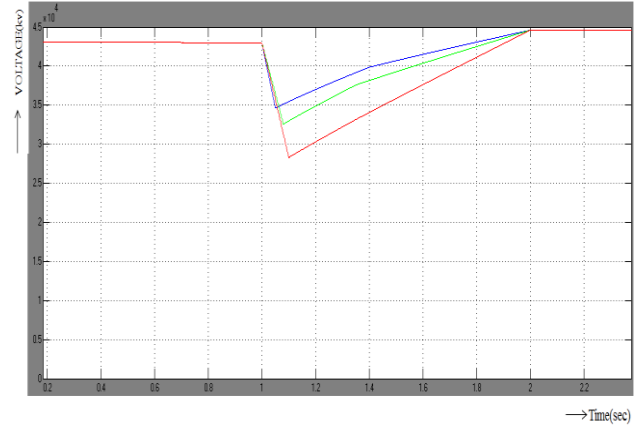


Fig 5(i)

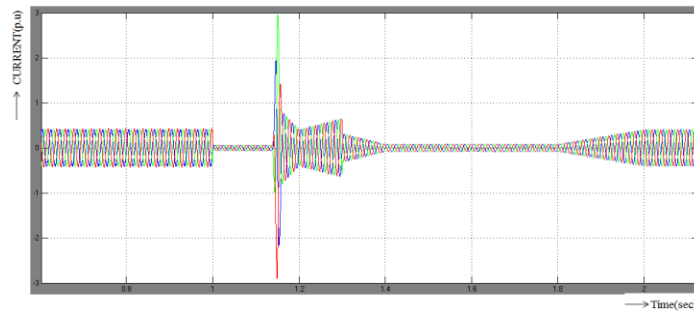


Fig 5(f)

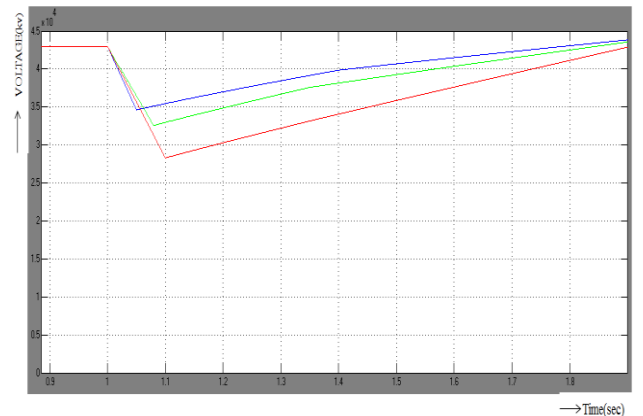


Fig 5(j).

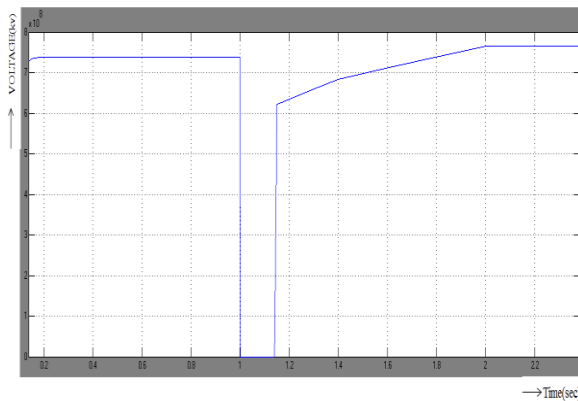


Fig 5(g)

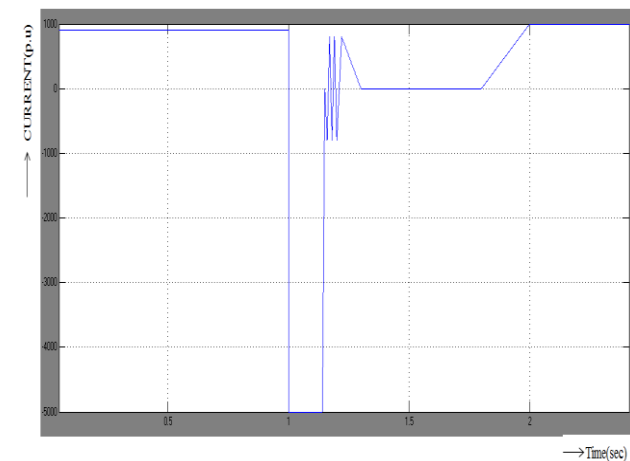


Fig 5(h)

Fig. 5. Waveforms demonstrating dc fault ride-through capability of HVDC transmission systems based on hybrid voltage multilevel converter with ac side cascaded H-bridge cells. (a) Active and reactive power converter 1 exchanges with . (b) Active and reactive power converter 2 exchanges with . (c) Voltage magnitude at . (d) Voltage magnitude at . (e) Current waveforms converter 1 exchange with grid at . (f) Current waveforms converter 2 exchange with grid at . (g) Converter 2 dc link voltage. (h) Zoomed version of dc link current demonstrating the benefits of dc fault reverse blocking capability. (i) Voltage across the H-bridge cell capacitors of converter 1. (j) Voltage across the H-bridge cell capacitors of converter 2.

Fig. 5 shows the results when the test network is subjected to a temporary solid pole-to-pole dc fault at the middle of the dc link. Fig. 5(a) and (b) shows the active and reactive powers that

converter stations 1 and 2 exchange with and . Observe zero active and reactive power exchange between the converter stations and ac grids and during the fault period, hence there is no current flow in the switches of converters 1 and 2. However, a large surge in active and reactive power is observed when the gating signals to converters 1 and 2 are restored after the fault is cleared, in order to restart the system. Fig. 5(c) and (d) shows that the current surge experienced by both converter stations causes noticeable voltage dipping at and due to increased consumption of reactive power during system start-up and dc link voltage build-up following fault clearance. The surge in active and reactive powers in both converter stations occurs as the dc side capacitors try to charge from both ac sides; this causes a large current flow from both ac sides to the dc side to charge the dc link capacitors and cable distributed capacitors as shown in Fig. 5(e) and 5(f). The results in Fig. 5(e) and 5(f) also demonstrate the benefits of dc fault reverse blocking capability inherent in this hybrid system, as the converter switches experience high current stresses only during dc link voltage build-up. Fig. 5(g) shows that converter 2 dc link voltage recovers to the pre-fault state after the fault is cleared. Notice the recovery period for the dc link voltage is relatively long; this is the major disadvantage of the proposed HVDC systems as it uses a common dc link capacitor. Fig. 5(h) expands the dc fault current and shows the 60-kA peak decays to zero in less than four cycles (for 50 Hz) after discharge of dc link and cable distributed capacitors. This result confirms the possibility of eliminating dc circuit breakers to isolate permanent dc side faults in dc networks that use HVDC converters with current limiting capability. Fig. 5(h) also shows the ac grids start to contribute to the dc link current after the fault is cleared, to charge the dc side capacitors. Fig. 5(i) and (j) shows the voltage across the 21 H-bridge cells of the converter stations 1 and 2 (each group of traces represent voltages across 7 H-bridge cell capacitors in each phase). The voltage across the

H-bridge cell capacitors remains unaffected during the entire fault period as the converters are blocked. The cell capacitors start to contribute energy to the main dc link capacitors during dc link voltage build-up after restoration of the converter gating signals. This contribution creates a noticeable reduction in the cell capacitor voltages during system restart. The cell capacitors of converter 2 that regulate dc link voltage, experience a larger voltage dip than converter 1, which regulates active power. However, the reduction in H-bridge cell capacitor voltages is minimized if large capacitance is used.

V. CONCLUSION

This paper has reviewed the present state of the art in multilevel converter technology by discussing the most recent contributions on topologies, modulation, and applications. At this point, it can be concluded that multilevel converters have reached a certain level of maturity, given their industrial presence and successful practical application. Nevertheless, the high amount of recent publications on the subject and the fact that the number of commercially available topologies has doubled in the past few years reveal that there is still plenty of room for further development. It is clear that the development of power electronic devices, the changes and evolution of the industrial processes, and new more demanding standards and regulations will drive and shape the future of multilevel converter technology.

The new generation VSC-HVDC transmission system based on a hybrid multilevel converter with ac-side cascaded H-bridge cells. The main advantages of the proposed

HVDC system are:

- potential small footprint and lower semiconductor losses compared to present HVDC systems.
- low filtering requirements on the ac sides and presents high-quality voltage to the converter transformer.
- does not compromise the advantages of VSC-HVDC systems such as four-quadrant operation;

voltage support capability; and black-start capability, which is vital for connection of weak ac networks with no generation and wind farms.

- modular design and converter fault management (inclusion of redundant cells in each phase may allow the system to operate normally during failure of a few H-bridge cells; whence a cell bypass mechanism is required).
- resilient to ac side faults (symmetrical and asymmetrical).
- inherent dc fault reverse blocking capability that allows converter stations to block the power paths between the ac and dc sides during dc side faults (active power between ac and dc sides, and reactive power exchange between a converter station and ac networks), hence eliminating any grid contribution to the dc fault current.

REFERENCES

1. G. P. Adam *et al.*, "Network fault tolerant voltage-source-converters for high-voltage applications," in *Proc. 9th IET Int. Conf. AC and DC Power Transmission*, London, U.K., 2010, pp. 1–5.
2. Y. Zhang *et al.*, "Voltage source converter in high voltage applications: Multilevel versus two-level converters," in *Proc. 9th IET Int. Conf. AC and DC Power Transmission*, London, U.K., 2010, pp. 1–5.
3. G. P. Adam *et al.*, "Modular multilevel inverter: Pulse width modulation and capacitor balancing technique," *IET Power Electron.*, vol. 3, pp. 702–715, 2010.
4. M. M. C. Merlin *et al.*, "A new hybrid multi-level voltage-source converter with DC fault blocking capability," in *Proc. 9th IET Int. Conf. AC and DC Power Transmission*, London, U.K., 2010, pp. 1–5.
5. V. Naumanen *et al.*, "Mitigation of high - originated motor overvoltages in multilevel inverter drives," *IET Power Electron.*, vol. 3, pp. 681–689, 2010.
6. H. Abu-Rub *et al.*, "Medium-voltage multilevel converters: State of the art, challenges, and requirements in industrial applications," *IEEE Trans. Ind. Electron.*, vol. 57, no. 8, pp. 2581–2596, Aug. 2010.
7. G. P. Adam *et al.*, "Modular multilevel converter for medium-voltage applications," in *Proc. IEEE Int. Conf. Electr. Mach. Drives Conf.*, 2011, pp. 1013–1018.
8. G. P. Adam, S. J. Finney, A.M.Massoud, and B.W.Williams, "Capacitor balance issues of the diode-clamped multilevel inverter operated in a quasi-two-state mode," *IEEE Trans. Ind. Electron.*, vol. 55, no. 8, pp. 3088–3099, Aug. 2008.
9. M. Chaves *et al.*, "New approach in back-to-back m-level diodeclamped multilevel converter modelling and direct current bus voltages balancing," *IET Power Electron.*, vol. 3, pp. 578–589, 2010.
10. N. Flourentzou *et al.*, "VSC-based HVDC power transmission systems: An overview," *IEEE Trans. Power Electron.*, vol. 24, no. 3, pp. 592–602, Mar. 2009.
11. L. G. Franquelo *et al.*, "The age of multilevel converters arrives," *IEEE Ind. Electron. Mag.*, vol. 2, no. 1, pp. 28–39, 2008.
12. U. N. Gnanarathna *et al.*, "Efficient modeling of modular multilevel HVDC converters (MMC) on electromagnetic transient simulation programs," *IEEE Trans. PowerDel.*, vol. 26, no. 1, pp. 316–324, Jan. 2011.
13. S. Kouro *et al.*, "Recent advances and industrial applications of multilevel converters," *IEEE Trans. Ind. Electron.*, vol. 57, no. 8, pp. 2553–2580, Aug. 2010.
14. G. P. Adam *et al.*, "Steady-state and transient performance of DC transmission systems based on HVDC technology," in *Proc. 9th IET Int. Conf. ACDC Power Transmission*, 2010, pp. 1–5.

15. D. Guanjun *et al.*, "New technologies of voltage source converter (VSC) for HVDC transmission system based on VSC," in *Proc. IEEE Power Energy Soc. Gen. Meeting—Conversion and Delivery of Electrical Energy in the 21st Century*, 2008, pp. 1–8.
16. N. Flourentzou and V. G. Agelidis, "Optimized modulation for AC-DC harmonic immunity in VSC HVDC transmission," *IEEE Trans. Power Del.*, vol. 25, no. 3, pp. 1713–1720, Jul. 2010.
17. D. Cuiqing *et al.*, "Use of VSC-HVDC for industrial systems having onsite generation with frequency control," *IEEE Trans. Power Del.*, vol. 23, no. 4, pp. 2233–2240, Oct. 2008.
18. Z. Huang *et al.*, "Exploiting voltage support of voltage-source HVDC," *Proc. Inst. Electr. Eng.—Gen., Transm. Distrib.*, vol. 150, pp. 252–256, 2003
19. G. Kalcon *et al.*, "HVDC network: Wind power integration and creation of super grid," in *Proc. 10th Int. Conf. Environ. Electr. Eng.*, 2011, pp. 1–4.
20. D. Hui *et al.*, "Analysis of coupling effects on overhead VSC-HVDC transmission lines from AC lines with shared right of way," *IEEE Trans. Power Del.*, vol. 25, pp. 2976–2986, 2010
21. B. T. Ooi and X. Wang, "Boost-type PWM HVDC transmission system," *IEEE Trans. Power Del.*, vol. 6, no. 4, pp. 1557–1563, Oct. 1991.
22. G. P. Adam *et al.*, "HVDC Network: DC fault ride-through improvement," in *Proc. Cigre Canada Conf. Power Syst.*, Halifax, NS, Canada, Sep. 6–8, 2011, pp. 1–8.
23. G. P. Adam *et al.*, "Dynamic behaviour of five-level grid connected modular inverters," in *Proc. 9th Int. Conf. Environ. Electr. Eng.*, 2010, pp. 461–464.
24. M. Perez *et al.*, "Predictive control of AC-AC modular multilevel converters," *IEEE*

Trans. Ind. Electron., vol. 59, no. 7, pp. 2832–2839, Jul. 2012.

25. J. Háfner and B. Jacobson, "Proactive hybrid HVDC breakers—A key innovation for reliable HVDC grids," in *Proc. Cigre Conf.*, Bologna, Italy, Sep. 13-15, 2011,

Author's Profile



Mr. M. Srinath was born in Andhra Pradesh, India. He received his B.Tech degree in Electrical and Electronics Engineering from, N.B.K.R Institute Of Science And Technology, Vidyanagar in 2013 and pursuing M.Tech degree in Power Systems from ASIT, Gudur, JNTU, Anantapur, Andhra Pradesh, India. His areas of interest in the field of power systems and HVDC transmission systems.

Email: srinath.mdr@gmail.com



Mr. G. Hari Krishna was born in Venkatagiri, Andhra Pradesh, India, in 1984. He received his B.Tech degree in Electrical and Electronics Engineering from kuppam Engineering College, Kuppam, A.P., in 2007 and M.Tech degree in Power Electronics from JNTU Anantapur in 2012. Presently he is working as Asst. Professor in Department of EEE, Audisankara Institute of Technology, Gudur, Andhra Pradesh, India. He was the academic project coordinator for Under

Graduate & Post Graduate students. His research interests include power electronics, electrical drives, HVDC and FACTS, particularly multilevel converters and their corresponding control systems.



Mr. M. Nagaraju was born in Andhra Pradesh, India. He received the B.Tech degree in Electrical and Electronics Engineering from JNT University, Hyderabad in 2002 and M.Tech degree in Electrical Power Systems from JNT University Ananthapur in 2008. He is currently pursuing the Ph.D. degree at the JNT University, Hyderabad, Andhra Pradesh, India. He had worked as an Assistant professor in the Dept of EEE in N.B.K.R.I.S.T Vidyanagar. worked as a Assistant professor in the Dept of EEE in Chadalawada Engg.college, Tirupathi. Worked as lecture in Govt Polytechnic,Gudur. Currently He is working as an Associate Professor at Audisankara Institute of Technology Gudur,AP. He was the academic project coordinator for Under-Graduate & Post Graduate students. His areas of interest are Power Quality ,FACTS, Reactive Power Control.

Email: nag707@gmail.com